

**RESEARCH PERFORMANCE PROGRESS REPORT**

**FEDERAL AGENCY:**

U.S. DOE/NETL  
NATIONAL ENERGY TECH LAB  
3610 Collins Ferry Road  
PO Box 880  
Morgantown, WV 26507-0880

**FEDERAL GRANT OR OTHER IDENTIFYING NUMBER BY AGENCY:**

**DE-FE0029059**

**PROJECT TITLE:**

Remote Methane Sensor for Emissions from Pipelines and  
Compressor Stations Using Chirped-Laser Dispersion Spectroscopy

**PI NAME:**

Mark Zondlo  
Associate Professor of Civil and Environmental Engineering  
Email: [mzondlo@princeton.edu](mailto:mzondlo@princeton.edu)  
Phone: (609) 258-5037  
Fax: (609) 258-2760

**CO-PI NAME:**

Gerard Wysocki  
Associate Professor of Electrical Engineering  
Email: [gwyssocki@princeton.edu](mailto:gwyssocki@princeton.edu)

**SUBMISSION DATE:**

October 31, 2017

**DUNS NUMBER:** 00-248-4665

**RECIPIENT ORGANIZATON:**

Princeton University  
Princeton, NJ 08544

**PROJECT/GRANT PERIOD**

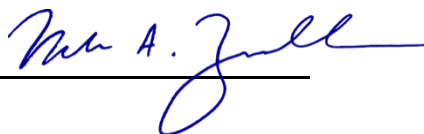
10/1/2016 - 3/31/2018

**REPORTING PERIOD END DATE**

September 30, 2017

**REPORTING TERM OR FREQUENCY**

Quarterly (for period 7/1/17 to 9/30/17)

  
\_\_\_\_\_

## Cover Page (previous)

### 2. Accomplishments

#### 2a. Goals

Leak rates of methane (CH<sub>4</sub>) from the natural gas supply chain result in lost profit from unsold product, public safety and property concerns due to potential explosion hazards, and a potentially large source of economic damages from legal liabilities. Yet large measurement challenges exist in identifying and quantifying CH<sub>4</sub> leak rates along the vast number and type of components in the natural gas supply chain. This is particularly true of the “midstream” components of gathering, processing, compression, transmission, and storage.

This project will develop and deploy new advances in chirped laser dispersion spectroscopy (CLaDS) to make an airborne-based sensor for remote detection of methane leaks from pipelines, compressor stations, and other midstream infrastructure. Leaks of methane not detected through routine pipeline patrols and only inferred by indirect methods (e.g. dead vegetation). The proposed heterodyne-enhanced chirped modulated CLaDS (HE-CM-CLaDS) system will offer ability to perform measurements with low light returns, immunity to back-scattered light intensity fluctuations and high linearity and extended dynamic range of concentration detection.

The proposed effort will use a range-resolved, integrated-path spectroscopic technique to remotely identify leaks along pipelines and other related facilities. The instrument will be capable of being deployed on a vehicle, manned aircraft, or making three-dimensional tomographic images with appropriate flight patterns of a microdrone or by passive sampling. Manned aircraft already patrol pipelines for threat detection and visible signs of leak on monthly timescales. Yet there exist no sensors that can show the necessary sensitivity to detect leaks from such a platform. In this project, we will develop, field test, validate, and demonstrate the system over a pipeline corridor. The system proposed here will target the following specifications:

- Open-path methane measurement
- Sensitivity to methane will be in the  $<1\text{ppmv}\cdot\text{m}/\text{Hz}^{1/2}$
- Simultaneous range measurement for 3D tomographic reconstruction
- Ability to perform sensitive CH<sub>4</sub> measurements by scattering from natural hard-targets

The technical innovation is using range-resolved, chirped modulation-chirped laser dispersion spectroscopic detection for methane quantification, which will provide the most robust yet relatively inexpensive hardware solution while delivering sensing performance needed for the target application. The proposed method utilizes optical phase of the detected light for molecular detection and thus is insensitive to fluctuations in intensity of backscattered light within four orders of magnitude, a key feature necessary when scanning through natural hard targets. The proposed system will be validated by controlled tracer releases when integrated onto vehicle and aircraft-based platforms.

Commercial translation to the marketplace will occur by partnering with a pipeline service provider, American Aerospace Technologies, Inc., for flight demonstrations to their clients in the gas, oil, and pipeline industries. In this way, feedback on the sensor performance and attributes

will be efficient and minimize delays in bringing the technologies to the private sector. Benefits of a commercial sensor with these capabilities include reductions of leaks for pipeline operators (more profit), earlier detection of leaks to avoid catastrophic explosion hazards (employee safety, public health and mitigation of property damage), and reduced methane emissions to the atmosphere (improving air quality).

## 2b. Major activities, results, and outcomes/achievements (Milestone Status Report at end)

### **Task 1: Project Management, Planning, and Reporting**

**Status:** Completed

**Deliverables:** Project Management Plan was March 20, 2017 and accepted by the Project Manager via email notification on March 27, 2017.

**Milestone A:** Data Management Plan submitted → milestone achieved on March 20, 2017.

### **Task 2: Development of HE-CM-CLaDS sensor**

**Milestone A:** System Developed → on track, planned by February 2018

#### **Research progress made in the last quarter:**

- **Collecting optics design with auto-focusing capability for UAV tracking**
- **Implementation of ranging capability in the FPGA based CLaDS system**

#### **Task 2.1: Auto-focusing collecting optics design for moving target**

In order to optimize optical signal reflected from a moving target on a UAV, the collecting optics needs to be designed to maximize optical power collection and allow automatic refocusing of the beam onto the fast photodetector (FPD). Figure 1a) shows a design of 3 lens system with high quality zoom relay which effectively focuses the light onto the FPD. Although the system can be optimized to be nearly diffraction-limited, it has a relatively long zoom length of 18 mm, and does not provide much space for a second optical channel for camera and the local oscillator channel planned for optical heterodyne enhancement. An alternative two lens system design shown in Figure 1b) uses an intermediate lens to defocus the return light into a nearly collimated beam, which can accommodate high quality optics needed in the imaging system. In addition to its simplicity, it has a zoom length of roughly 5 mm, which is more suitable for our UAV tracking needs.

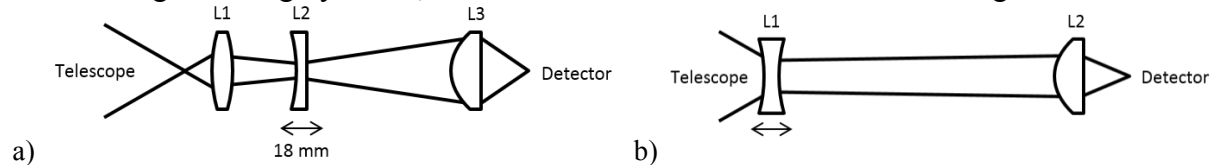


Figure 1. a) Zoom relay system using three lenses which reimage the focus of the telescope and b) zoom optic system which re-collimates the beam depending on object location.

To test the two-lens system, we take images through the telescope without and with the two-lens system in place. When the two-lens system is not included, the focused image shows high quality with sharp contrast (Figure 2a). After adding the re-collimating and focusing lenses, the image has increased magnification and suffers chromatic aberration as shown in Figure 2 b). Potential

solutions to the chromatic aberration including optical filtering and/or using customized lenses instead of off-shelf components will be tested in the next quarter.

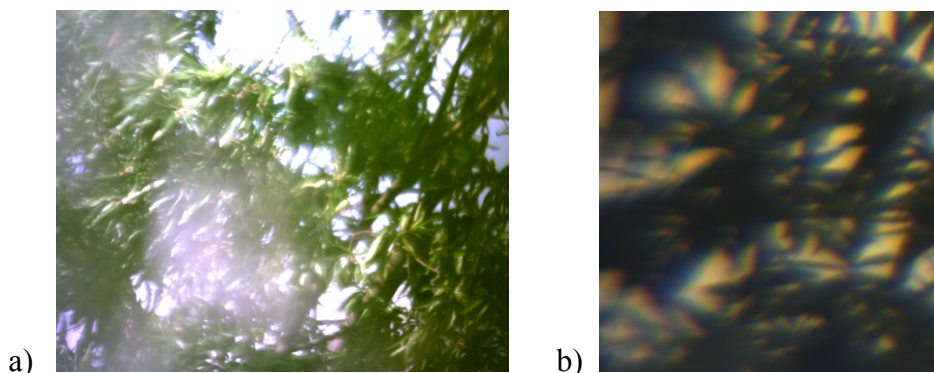


Figure 2. Imaging through telescope a) without and b) with relay optics.

The two-lens design will be integrated with the collecting optics for conventional CLaDS system and HE-CLaDS are shown in Figure 3. The movable re-collimating lens is placed right next to the telescope. A dichroic beamsplitter (BS) separates the probing NIR signal to the FPD from the visible signal to the camera. The second lens is placed before the FPD to refocus the light. For HE-CLaDS system, a second BS is added to allow the optical LO to co-align with the probing beam. A pair of lenses are used to refocus the two paths on a balanced FPD.

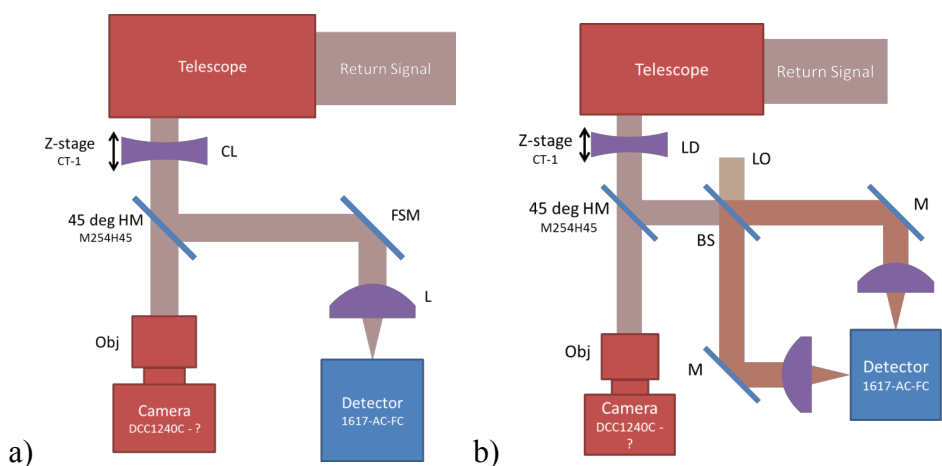


Figure 3. Collecting optics for a) CLaDS and b) HE-CLaDS with auto-focusing signal provided by the camera.

## Task 2.2: CLaDS ranging implementation

The dispersion signal obtained using CLaDS is a path-integrated measurement. In order to retrieve concentration of methane at a given location, differential measurements must be taken with optical path length measurement simultaneously. Our proposed solution to the problem is to integrate FM-CW radar with the optical spectroscopic measurement. In conventional CLaDS, multiple optical frequencies with a fixed RF frequency spacing are sent out to probe the target molecular species simultaneously. The return light forms a heterodyne beatnote at the given RF frequency on the photodetector. In order to measure the optical path length, or equivalently the time delay caused by propagation of the light over a given distance, a linear chirp is added to the RF frequency

spacing between the optical frequencies. The schematic of a simplified in-lab CLaDS ranging system is shown in Figure 4 a).

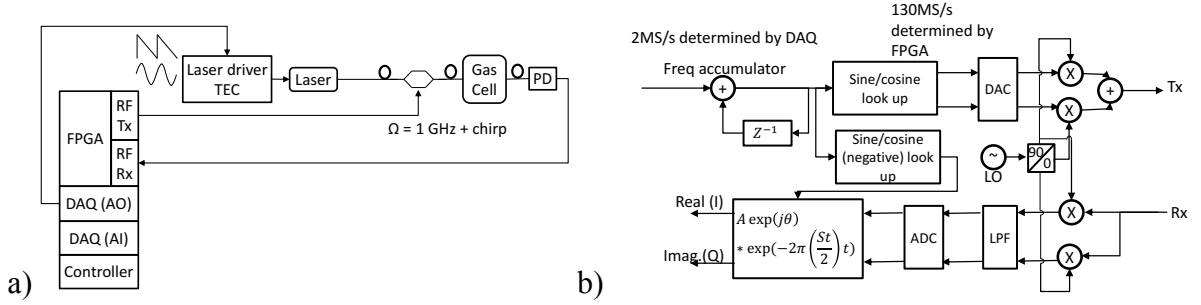


Figure 4. a) Fiber coupled CLaDS setup with ranging capability and b) FPGA transceiver design

Consider the initial RF spacing at  $\Omega_0$  Hz and a linear RF chirp rate of  $S_{RF}$  Hz/s, the linearly chirped RF signal will be in the form of

$$T_x(t) = A_T \cos\left[2\pi\left(\Omega_0 t + \frac{S_{RF} t^2}{2}\right)\right] \quad (1)$$

After the optical frequencies propagate over distance  $L$  at speed of light, the heterodyne beatnote after the photodetector becomes

$$R_x(t) = A_R \cos\left[2\pi\left(\Omega_0(t - \tau) + \frac{S_{RF}(t - \tau)^2}{2}\right)\right] \quad (2)$$

, where  $\tau = \frac{L}{c}$  is the time delay. After mixing  $R_x$  signal with  $T_x$  signal and demodulating for the phase, the phase difference between  $R_x$  and  $T_x$  is obtained as

$$\phi(t) = 2\pi\left(-S_{RF}\tau t + S_{RF}\tau^2 - \Omega_0\tau + S_{\phi}(t - \tau)\right) \quad (3)$$

The derivative of the fourth term is the conventional CLaDS signal that carries spectroscopic information. The first term corresponds to a frequency offset of  $S_{RF}\tau$ . The remaining two terms correspond to a phase offset. Both the frequency offset and the phase offset can be used to extract the time delay and corresponding distance.

A field-programmable gate array (FPGA) is used to implement all functions of the CLaDS system in a single data acquisition and control system. During the last quarter we have implemented ranging capability using the FPGA platform. The system is equipped with an RF adapter that provides a local oscillator (LO) whose frequency can be varied between 200 MHz and 4.4 GHz. Direct analog tuning of the LO frequency is slow and cannot reach the desired chirp rate above 100 MHz/s. The solution is to generate the linear chirp in the baseband using direct digital synthesizer (DDS) and then upconvert the signal to the RF band:

$$T_x(t) = A_T \sin(2\pi\Omega_0 t) \sin(2\pi \frac{S_{RF} t^2}{2}) + A_T \cos(2\pi\Omega_0 t) \cos(2\pi \frac{S_{RF} t^2}{2}) \quad (4)$$

Here  $\sin(2\pi \frac{S_{RF} t^2}{2})$  and  $\cos(2\pi \frac{S_{RF} t^2}{2})$  are generated digitally and converted to analog through DAC at 130 MHz sampling clock, whereas  $\sin(2\pi\Omega_0 t)$  and  $\cos(2\pi\Omega_0 t)$  are the in-phase and in-

quadrature parts of the local oscillator provided by the RF adapter, and the multiplication is achieved using the analog frequency mixer.

Correspondingly, the phase demodulation is also carried out in the baseband after the time delayed signal is received:

$$R_X[n] = -iI_R[n]\sin(2\pi \frac{S_{RF}(nT)^2}{2}) + Q_R[n]\cos(2\pi \frac{S_{RF}(nT)^2}{2}) \quad (5)$$

, where  $Q_R[n]$  and  $I_R[n]$  are digitized in-quadrature and in-phase signals downconverted from the received RF signal. A simplified block diagram of the chirp generation and demodulation is shown in Figure 4b).

For an ideal signal generation and demodulation in (4) and (5), the in-quadrature and in-phase components must be synchronized without phase skew or amplitude imbalance. To test the hardware, we generate a simple sinewave at 30 kHz in the baseband, which is expected to give a 30kHz frequency shift from the 1GHz local oscillator frequency at the transmitter.

The RF spectra of frequency shifted  $T_X(t)$  are shown in Figure 2. The spectrum in black shows the local oscillator frequency at 1GHz. When a frequency shift of 30 kHz is added, multiple harmonics at  $-f_0, -2f_0, 2f_0, 3f_0$  and the pick-up frequency show up in the red plot. The negative harmonics are dominant, with  $-f_0$  only 20 dB below the main frequency. To suppress the dominant harmonic, we introduce a phase shift in the baseband signal to pre-correct the phase skew. The improved spectrum is shown in Figure 2b).

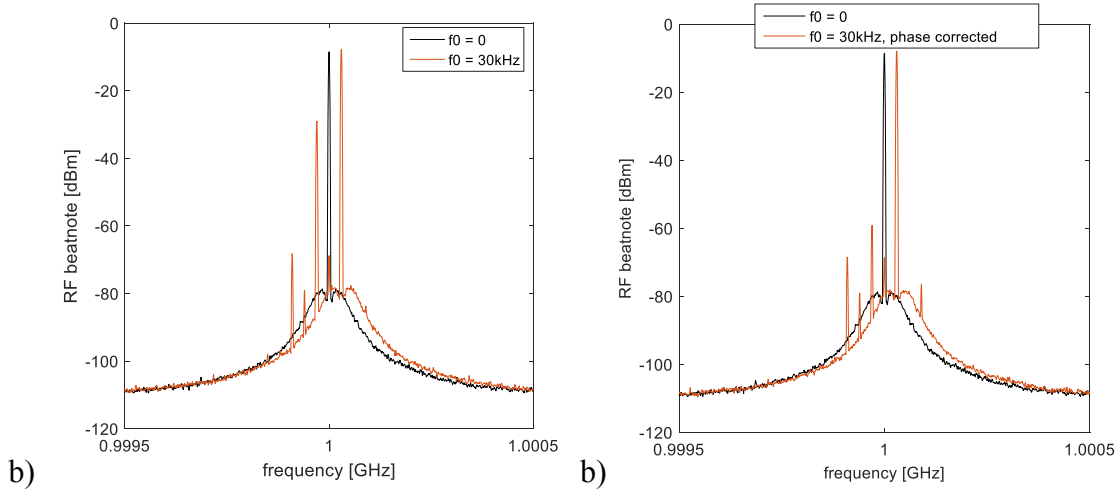


Figure 5. Digital frequency modulation a) before and b) after first harmonic suppression using phase correction.

The presence of harmonics severely distorts the CLaDS spectrum as a result of FM demodulation error as shown in Figure 6a). After correcting for the phase skews in the frequency shift, we are able to generate linear chirp in RF frequency at 290 MHz/s and sweeps over 29 kHz every 0.1ms in synchronization with 10kHz laser frequency modulation.

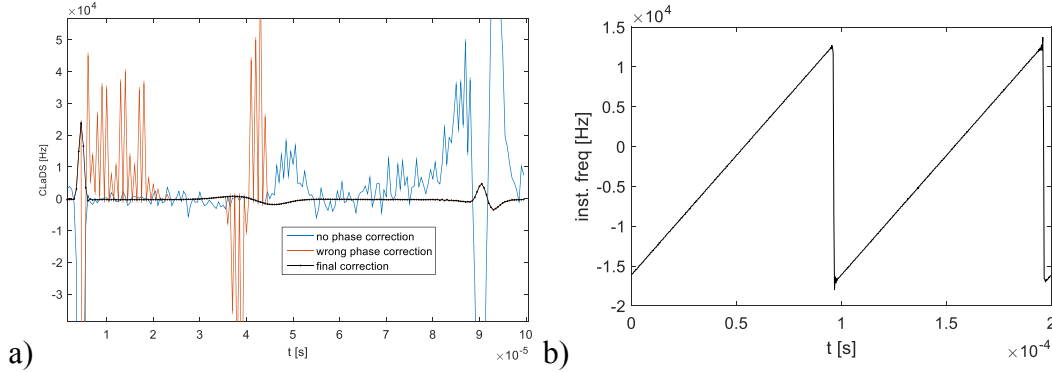


Figure 6. a) Demodulated CLaDS signal without (blue), with wrong (red) and correct (black) phase correction in RF transmission signal. b) Linearly chirped RF frequency after correction

### Task 3: Laboratory testing of system parameters

Status: In-progress

#### Research progress made:

- Laboratory testing of the ranging capability with CM-CLaDS

#### Task 3.1: In-lab ranging test with CM-CLaDS

The ranging capability implemented in Task 2.2 is compatible with variations of CLaDS techniques. When combined with chirp-modulated (CM) CLaDS, where the laser wavelength is modulated by a sinewave, the demodulated zeroth order harmonic of CLaDS signal is equal to the frequency offset created by the RF frequency chirp and time delay.

To test the implemented ranging functionality, fibers of 0.35m, 2m and 85m are inserted in the optical path after the EOM in the setup shown in Figure 4 a). A 20% CH<sub>4</sub> fiber coupled gas cell of length 3cm is added in series with the delay lines to provide spectroscopic reference. The reference signal for distance calibration is taken when no fiber delay line is inserted, and the path length difference is back calculated from the frequency offset difference and chirp rate at 250 MHz/s.

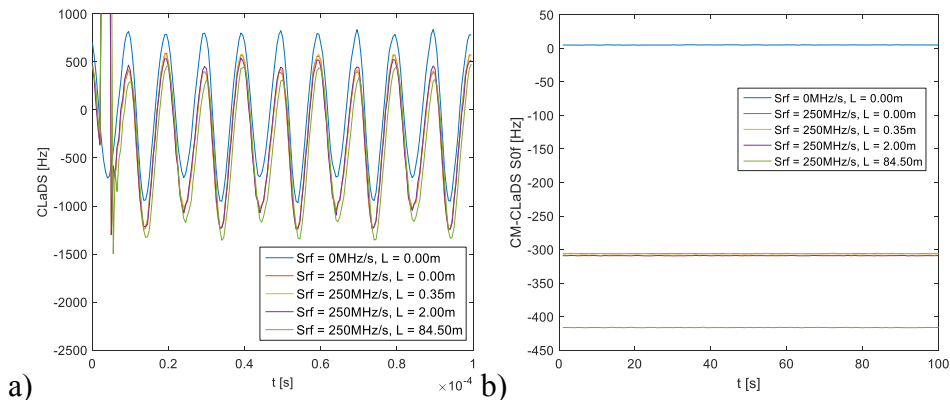


Figure 7. a) Demodulated CM-CLaDS signal with frequency offset b) 0<sup>th</sup> order harmonic of CM-CLaDS

The measurement results are summarized in Figure 7. The frequency demodulated CLaDS signals shown in Figure 7a are visibly downshifted due to different path delays. Figure 7b) shows the extracted zeroth order harmonic from Figure 7a) over a period of 100 s. A preliminary

retrieval of the distances yielded distances of 0.33m, 2.62 and 91.92m correspondingly, which is in reasonable agreement with the expected values. Due to the refractive index in fiber and uncertainty in determining the exact length of the fiber spool, a free-space test will be performed in the next quarter.

***Task 4: outdoor testing and validation of system performance***

Status: Not started yet, planned for November 2017

***Task 5: Development of tomographic reconstruction algorithms***

Status: Not started yet, planned for August 2018

***Task 6: Mobile field tests***

Status: Not started yet, planned for October 2018

***Task 7: Drone-based reflector target imaging***

Status: Not started yet, planned for January 2019

***Task 8: Airborne flight measurements***

Status: Not started yet, planned for July 2019

**Milestone Status Report**

Milestone Title / Description	Planned completion	Actual completion	Verification method	Comments
A: Data management plan submitted	3/31/17	3/27/17	Accepted by program manager.	
B: system developed	2/28/18			
C: Lab testing completed	8/31/18			
D: Field validation completed	10/31/18			
E: Tomographic algorithms	10/31/19			
F: Mobile field data collected	1/31/19			
G: Drone-based flights	9/30/19			
H: Manned aircraft flights	2/28/20			

Note: all dates extended by 5 months due to delays in paperwork at start but consistent with the timeframes in the SOPO with an effective start date of 3/1/17.

**2c. Training and development**

Not requested.

**2d. Dissemination of Results / Outreach**

No outreach events have occurred to communities of interest.



## **2e. Plans for Next Reporting Period**

In the next reporting period we plan to finalize the design of the receiver optics based on Newtonian reflectors and auto-focusing optics. Additionally a series of tests and optimization of the ranging functionality of the CLaDS system is planned to be performed in the next quarter.

## **3. Products**

### **Publications, conference papers, and presentations**

#### **Publications**

G. Plant, Y. Chen, and G. Wysocki, "Optical heterodyne-enhanced chirped laser dispersion spectroscopy," *Optics Letters* 42, 2770-2773 (2017).

#### **Books or other non-periodical, one-time publications**

None.

#### **Other publications, conference proceedings, and presentations**

Y. Chen, G. Plant, and G. Wysocki, "Heterodyne Efficiency in Chirped Laser Dispersion Spectroscopy," in Conference on Lasers and Electro-Optics(Optical Society of America, San Jose, California, 2017), p. SW4L.5.

## **4. Participants and other collaborators**

American Aerospace Technologies Inc., the commercial partner that will be flying the sensor on aircraft in Year 3 and who will fly a drone with a reflecting target in Year 2, has provided advice on aircraft constraints. These constraints play important roles in the overall design of the sensor while there is still time to adjust to any payload issues (or orientation).

## **5. Impact (optional)**

Nothing to report at this time.

## **6. Changes/problems**

No changes to the SOPO or technical problems have been encountered. All tasks and milestones remain on schedule and on specification.

## **7. Special reporting requirements**

Appendix A: Test plan for Tasks 3 and 4

Appendix B: Plant et al., *Optics Letters* publication

Appendix C: Chen et al., CLEO Conference Proceedings

## **8. Budgetary information**

Follows on next pages.

**Appendix A: Test Plan for Task 3 and Task 4**

**Test Plan for**

**Task 3** “Laboratory testing of system parameters”  
and **Task 4** “Outdoor testing and validation of system performance”

**SUBMITTED TO**  
U.S. DOE/NETL  
NATIONAL ENERGY TECH LAB  
3610 Collins Ferry Road  
PO Box 880  
Morgantown, WV 26507-0880

Email: [FITS@NETL.doe.gov](mailto:FITS@NETL.doe.gov)

CC: [Robert.Vagnetti@NETL.DOE.GOV](mailto:Robert.Vagnetti@NETL.DOE.GOV) and [Angela.Bosley@NETL.DOE.GOV](mailto:Angela.Bosley@NETL.DOE.GOV)

**PROJECT TITLE**

Remote Methane Sensor for Emissions from Pipelines and  
Compressor Stations Using Chirped-Laser Dispersion Spectroscopy

**FEDERAL GRANT OR OTHER IDENTIFYING NUMBER BY AGENCY:**

**DE-FE0029059**

**PI NAME**

Professor Mark Zondlo  
Email: [mzondlo@princeton.edu](mailto:mzondlo@princeton.edu)  
Phone: (609) 258-5037

**CO-PI NAME**

Professor Gerard Wysocki  
Email: [gwyssocki@princeton.edu](mailto:gwyssocki@princeton.edu)  
Phone: (609) 258-8187

**SUBMISSION DATE**

October 31, 2017

**DUNS NUMBER:** 00-248-4665

**RECIPIENT ORGANIZATION**

Princeton University  
Princeton, New Jersey 08544

**PROJECT/GRANT PERIOD**

10/1/2016 - 3/31/2018

### **Test Plan – Task 3 “Laboratory testing of system parameters”**

In this task all system functions and the system performance will be tested and quantified.

There will be three main functions of the heterodyne-enhanced chirped laser spectroscopy (HE-CLaDS) system for methane detection that will be tested, those include: 1) spectroscopic methane sensing; 2) range measurement; and 3) mobile target (UAV) tracking capabilities. We are planning to perform separate testing of these functions in the laboratory conditions as well as a complete system test that will provide all three capabilities simultaneously. Below is a detailed outline for the “Laboratory testing of system parameters”:

#### **3.1) Spectroscopic methane sensing with HE-CLaDS**

- a. Evaluation of the methane concentration measurement precision (sensitivity).
- b. Evaluation of the methane concentration measurement accuracy and long-term system drift.
- c. Evaluation of heterodyne enhancement

#### **3.2) Range (distance) measurement**

- d. Evaluation of the range measurement precision and accuracy.

#### **3.3) Mobile target (UAV) tracking capabilities**

- e. Evaluation of auto-focusing system (z direction)
- f. Evaluation of lateral object tracking (x and y direction).

In the following text we provide detailed description of procedures and quantitative performance analysis that will be used to achieve the proposed goals of the project.

#### **3.1) Spectroscopic methane sensing with HE-CLaDS**

Testing of the spectroscopic methane sensing capabilities will be performed in two distinct measurement setups: i) HE-CLaDS system equipped with a fiber-coupled gas cell containing a calibrated methane gas mixture; and ii) free-space HE-CLaDS stand-off system in the laboratory with an on-site point methane sensor used for calibration. In both settings both the system precision (1a) and accuracy (1b) will be evaluated using the following procedures:

##### 3.1a) Evaluation of the methane concentration measurement precision (sensitivity).

Evaluation of the system precision will be performed in the measurement setups (i) and (ii) by implementing a spectral scan across the target methane transition followed by a fitting of spectroscopic model using HITRAN Database parameters. Fit residuals will be used for quantitative analysis of a noise observed at a single spectral point, which is representative of the performance of the system operated in a line-locked mode (laser frequency locked to the center of the target transition) while providing information about other system parameters (such as chirp-rate, symmetry of the modulation sidebands, scan linearity etc.) . The measurement precision will be reported using path- and bandwidth-normalized units (ppmv-m/Hz<sup>1/2</sup>, parts-per-million by volume of methane times meter related to the optical path used in setup (i) and (ii) respectively and normalized to the measurement bandwidth in Hz).

##### 3.1b) Evaluation of the methane concentration measurement accuracy and system drift.

Evaluation of the system accuracy and long-term drift will be performed in a line-locked mode of the HE-CLaDS system, in which the laser frequency will be actively controlled and set to the center of the target methane transition. Evaluation of the system accuracy and drift will be performed in the measurement setups (i) and (ii). In the measurement system (i) a calibration gas mixture of methane in nitrogen (traceable to the NIST standards) will be used as the reference for determination of the system accuracy. In the measurement system (ii) a commercial point methane sensor (LICOR LI-7700 analyzer) calibrated by World Meteorological Organization standards near ambient levels (for  $\text{CH}_4 \leq 2500$  ppbv, the accuracy will be  $<10$  ppbv) and NIST-traceable standards at higher values (for  $\text{CH}_4 > 2.5$  ppmv, 10% accuracy) will be used as the reference for estimation of the system accuracy in standoff detection mode. A more controlled accuracy measurement in a standoff detection mode will be performed in task 4 using a dedicated calibration facility planned in this task.

### 3.1c) Evaluation of heterodyne enhancement.

Evaluation of the heterodyne enhancement in HE-CLaDS will be performed by comparison of the carrier-to-noise measurements of the photo-detected radio frequency (RF) heterodyne signal in the conventional CLaDS as well as HE-CLaDS. The power in the signal channel will be preserved in both configurations enabling direct evaluation of the enhancement. The measurements will be performed for a different levels of returning power (ranging from microwatts down to the detection limit expected at the level of single nano-Watts) adjusted by neutral density optical filters. Studies of heterodyne efficiency will be conducted performing a series of experiments involving different scattering materials as the targets (e.g. sand-blasted aluminum plate, retro reflecting tape, wood, painted surfaces etc.) and the results will be compared with the results obtained with neutral density filters for both conventional CLaDS as well as HE-CLaDS.

## 3.2) Range (distance) measurement

Testing of the range (distance) measurement capability will be performed in two distinct measurement setups: i) short-distance (1-3m) with a reflecting target installed on a distance-adjustable optical rail; and ii) long-range (30-100m) measurement. In both settings both the system range measurement precision (2a) and accuracy (2b) will be evaluated using the following procedures:

### 3.2a) Evaluation of the range measurement precision and accuracy.

Measurement precision in both measurement setups (i) and (ii) will be evaluated by statistical analysis of repetitive distance measurements performed at the same target positions. The accuracy and range measurement drift will be evaluated by acquiring a long-term time sequence of distance measurements at the same target location and by post processing of the data using Allan deviation analysis. In the short-distance measurement setup (i) the target will be placed on a translation stage mounted on the optical rail and measurements will be performed at different positions of the target (within 1-3m range). The position of the target will be determined with sub-cm precision using a tape measure. In the long-distance measurement setup (ii) the target will be placed on a tripod and measurements will be performed at different positions of the target ranging from 10m to 100m. The position of the target will be determined with a commercial laser range finder (Leica Disto D8) providing  $\pm 1\text{mm}$  accuracy at a distance of 10m. For distances  $>30\text{m}$  the maximum deviation increases to  $\pm 0.15\text{mm}$  per meter of the measured range (at the maximum

range of 100m the maximum deviation should not exceed  $\pm 15\text{mm}$ , which is well below our target HE-CLaDS system accuracy of  $<0.1\text{m}$ )

### **3.3) Mobile target (UAV) tracking capabilities**

Testing of the mobile target (UAV) tracking will be performed in two stages. In stage 1 we will test the auto-focusing system required to adjust the collection telescope optics to track the mobile target in z-direction (away from telescope). In stage 2 we will test the lateral object tracking that is required to track the mobile target in x- and y-direction. The following procedures will be used to perform in-laboratory testing:

#### **3.3a) Evaluation of auto-focusing system (z direction).**

Evaluation of the auto-focusing system will be performed in the stand-off detection configuration similar to the long-range test in point 2a. The test will be performed at different stand-off distances selected between 30m and 100m. The depth of focus will be determined at each distance. The target will be placed at different positions separated by a distance larger than this defined by the depth of focus. The developed autofocus algorithm will be executed and the efficiency and the time required to re-focus the collection optics will be measured at each stage of the development process. We will also test auto-focusing tracking capability of a continuously moving target, and the maximum speed of the object at which the auto-focusing system provides reliable tracking will be determined and recorded. The optimum auto-focusing methodology will be identified and implemented in the final version of the sensor system prototype.

#### **3b) Evaluation of lateral object tracking (x and y direction).**

Evaluation of the lateral object tracking will be performed in the stand-off detection configuration similar to the long-range tests in point 2a and 3a. The test will be performed at different stand-off distances selected between 30m and 100m and will be restricted to the actual field of view off the collection optics. The target will be placed at different distances from the instrument and will be translated in x and/or y direction using motorized translation stage. The developed object tracking algorithm will be executed to control the large-aperture gimbal mirror in front of the telescope used to redirect and track the target at the stand-off distance. The efficiency and the time required to redirect the collection optics to a new target position will be measured at each stage of the development process. We will also test tracking capability of a continuously moving target, and the maximum speed of the object at which the lateral object tracking system provides reliable tracking will be determined and recorded. The optimum lateral object tracking methodology will be identified and implemented in the final version of the sensor system prototype.

## **Test Plan – Task 4 “Outdoor testing and validation of system performance”**

This task will demonstrate system performance outside in a field environment with a goal of quantifying precision, accuracy, and range resolution. First, an outdoor calibration facility will be constructed to accurately determine a known amount of CH<sub>4</sub> along a pre-defined optical path. Second, controlled releases of CH<sub>4</sub> will be made along the optical path to show path-integrated concentration measurements with simultaneous range determination, accuracy, and overall precision as a function of back-reflected light.

### **4.1) Develop 100 m round-trip outdoor calibration system**

This task will involve the temporary construction of a 50 m long, ~ 15 cm diameter tube (likely PVC or similar) in which a known flow of gas can be added at different points along the enclosure. A hard surface target (e.g. 30 cm x 30 cm board that can be used to adjust reflectivity, e.g., by placing an aluminum square on it, fully reflective mirror, board with grass/dirt, etc.) will be located at the end of the tube. A large industrial grade fan/pump will exhaust the air at a port near the end of the tube. The inside of the tube will be painted black to minimize scattered light. Ambient air will be drawn through a port near the start of the tube at rates of 0.1-0.01 m<sup>3</sup> s<sup>-1</sup>, and the sensor optical head will be located at this end as well. The air will have a residence time of 9-90 s inside the tube and a mean flow speed of 0.6-6 m s<sup>-1</sup>. A LICOR LI-7500 CH<sub>4</sub> sensor will read the CH<sub>4</sub> concentrations at the input air and will be used to confirm the gas standard mixtures. Ports will be built every 10 m to add known amounts of CH<sub>4</sub> from a calibrated cylinder at the source, the process of which will be described below. These flow rates will ensure turbulent mixing of the plume rapidly downstream of the input point.

### **4.2) Calibrate sensor precision, accuracy, and resolution at differing backscatter**

We envision two types of tests: static tests where the air is isolated inside the tube and dynamic (flowing) tests that allow introduction of gas standards at different distances.

With the outdoor calibration facility noted above, the static tests will be conducted over a range of target reflectivity (backscattered light) and CH<sub>4</sub> concentrations. The backscatter targets will be surfaces that go from fully reflective (e.g. mirror) to ones that are more consistent with the environment (e.g. grass/soil or sand). The front and back ends of the calibration tube will be sealed in these experiments but remain at ambient temperatures and pressures. The goal is to demonstrate the sensitivity over four orders of magnitude of backscattered light (fully reflective, ~ 10%, 1%, and 0.1% and 0.01% of the fully a reflective surface). These studies will be conducted at two different concentrations-pathlengths to show relevance near the detection limit and at more typical ambient levels. First, we will use ambient CH<sub>4</sub> in air to yield a signal of ~ 200 ppmv-m (about 200:1 SNR at the expected precision), followed by a 20 ppmv CH<sub>4</sub> in air standard to yield an integrated pathlength of 2000 ppmv-m. Note that 2000 ppmv-m is consistent with an airplane flying 500 m above a pipeline and scanning toward the ground at ambient CH<sub>4</sub> concentrations (500 m x 2 (roundtrip) x 2 ppmv CH<sub>4</sub> ambient). The static tests allow for controlled tests of the instrument precision and absolute calibration over a range of backscattered targets and relevant (though uniform) concentrations.

For dynamic experiments, we will flow ambient air into the calibration tube on the sensor end and add known amounts of CH<sub>4</sub> at different distances along the calibration tube (at 10, 20, 30, and 40 m from the end). These experiments will test the sensitivity to detecting a higher concentration plume at different distances from the sensor. For these tests, we will use a backscattered surface that has a target reflectivity of 0.1-1% of a fully reflective surface. Ambient air will be drawn into the tube at the start via a large pump/fan on the downstream end. A LICOR LI-7700 sensor will measure the input CH<sub>4</sub> concentrations in

air, and these concentrations will be confirmed on the downstream side when the CH<sub>4</sub> standards is mixed with ambient air. A flow meter will record the total volumetric flow of air on the downstream side. A high concentration of CH<sub>4</sub> (e.g. 1000 ppmv) will be added to each of the ports individually. The flow rate of ambient air will be much greater (factor of 2) than the total flow, ensuring that the mixed air remains largely downstream of the input location. The gas standard will be added at each of the input ports, and the flow rate (dilution) will be adjusted to achieve an equivalent path integrated concentrations of 500 and 2000 ppmv-m but with the standard added at each of the distances (i.e. 10, 20, 30, and 40 m downstream of the sensor). These tests will demonstrate the uniformity of the sensor readings across the pathlength.



# Optics Letters

## Optical heterodyne-enhanced chirped laser dispersion spectroscopy

GENEVIEVE PLANT,<sup>†</sup> YIFENG CHEN,<sup>†</sup> AND GERARD WYSOCKI\* 

Electrical Engineering Department, Princeton University, Princeton, New Jersey 08544, USA

\*Corresponding author: gwyssocki@princeton.edu

Received 26 May 2017; accepted 13 June 2017; posted 19 June 2017 (Doc. ID 295883); published 11 July 2017

**A proof-of-concept heterodyne-enhanced chirped laser dispersion spectroscopy system is presented. In remote sensing systems where low return powers are expected, the addition of an optical local oscillator and subsequent nonlinear processing can provide improved performance in chirped laser dispersion spectroscopy. Details about the system configuration, phase noise cancellation, and experimental verification are discussed.** © 2017 Optical Society of America

**OCIS codes:** (300.6310) Spectroscopy, heterodyne; (300.6390) Spectroscopy, molecular; (260.2030) Dispersion.

<https://doi.org/10.1364/OL.42.002770>

Spectroscopic techniques that can be applied to remote, open-path trace-gas sensing configurations are of importance for studies of large-scale trends, monitoring of large regions, or detection of potentially hazardous areas. In such configurations, the sensing environment is uncontrolled and susceptible to external noise sources such as atmospheric turbulence. Dispersion techniques are of particular interest in these configurations because the spectroscopic signal is encoded into the phase of the received light. Therefore, intensity noise introduced by turbulence or other sources does not directly translate into signal fluctuations. Atmospheric turbulence does, however, introduce phase noise to the transmitted light. This issue is mitigated in several techniques by the co-propagation of two (or more) signals and a differential measurement scheme [1–3] and in a frequency-comb-based system by transmitting only a single comb, while leaving the second comb to act as a strong local oscillator and numerically correcting for the turbulence-induced phase noise [4]. One of the techniques that takes advantage of a differential measurement with co-propagating waves is chirped laser dispersion spectroscopy (CLaDS), which probes optical dispersion induced by the presence of the targeted molecules [3]. By measuring optical dispersion, CLaDS offers potential advantages over conventional open-path, absorption-based techniques, namely, the linearity between the measured dispersion and the sample concentration [5], and the immunity to intensity/amplitude fluctuations [6]. While turbulence-induced phase noise is mitigated in co-propagation techniques such as CLaDS, the total return power

in these systems is relatively low and typically far below the saturation limit of the photodetector. The use of these attenuated signals in a differential heterodyne measurement limits the overall heterodyne gain of the detection scheme. In this Letter, we investigate a sensing configuration that preserves the phase-noise cancellation by co-propagation of a multifrequency signal, while offering the heterodyne gain through use of a strong optical local oscillator and subsequent nonlinear mixing. The proof-of-concept experiment discussed here demonstrates the proposed sensing architecture and signal-processing scheme as well as verifies the phase noise cancellation property and demonstrates an improvement in signal-to-noise ratio (SNR) via heterodyne enhancement of weak signals.

Here we present a methodology to improve the sensitivity of a CLaDS instrument in the limit of low light returns by adding a strong optical local oscillator. CLaDS provides a measure of optical dispersion resultant from the interaction of laser light with the molecular transitions of a target species. To probe optical dispersion, a multi-frequency {e.g., single-sideband (SSB) or dual-sideband (DSB) [7]} beam is generated with a well-defined frequency spacing,  $\Omega$ . When the different frequency components interact with the resonant transition, each component experiences a different index of refraction. The addition of a chirped laser frequency provides significant enhancement of the dispersion signal due to the derivative nature of the technique. At the detector, optical heterodyne detection is performed and the dispersion signal is retrieved through demodulation of the instantaneous frequency of the beatnote signal. The CLaDS signal amplitude is directly proportional to the species concentration, which can be determined through predetermined calibration or spectral fitting.

Rejection of turbulence-induced phase noise is achieved through co-propagation of the multi-frequency beam through the sample. Assuming that the frequency dependency of the various noise sources is not significant over the relatively small frequency spacing of the probe frequencies ( $\Omega \ll \omega$ ), the turbulence noise can be considered a common mode between the frequency components. This correlated noise is then rejected through the differential processing of the received signals. The total output noise in a CLaDS measurement is determined by the noise present at the input of the frequency demodulator. Assuming a white amplitude noise at the demodulator input, given by the power spectral density  $N_i$  ( $A^2/\text{Hz}$ ), the process of



ideal frequency demodulation results in an output noise power spectral density given by Eq. (1) for a given carrier amplitude,  $A$  [8]:

$$S_o(f) = \frac{N_i}{A^2} f^2, \quad \text{for } |f| < B. \quad (1)$$

The output noise of the demodulator, and therefore the noise in the CLaDS signal, is subsequently calculated by integrating the noise power spectral density over the signal bandwidth,  $B$ . The result of which is given in Eq. (2):

$$\sigma_{\text{CLaDS}} = \sqrt{\frac{N_i \cdot B^3}{3A^2}} = \sqrt{\frac{B^2}{6 \cdot \text{CNR}}}. \quad (2)$$

For a given carrier-to-noise ratio ( $\text{CNR} = A^2/(2N_i B)$ ) and bandwidth at the input of the detection system, the noise in the CLaDS measurement can be modeled according to Eq. (2) [9,10]. Assuming the same detection bandwidth,  $B$  (which is determined by the chirp rate and signal strength), Eq. (2) shows that the output noise in the CLaDS signal can be reduced through an increase in the CNR of the received RF beatnote signal. This increase can be achieved through a reduction of the detection noise or increase in the carrier power. The former approach was the focus of several previous works, which aimed at lowering the detection bandwidth and corresponding noise, through the use of downconversion techniques and slower detection systems [11,12]; however, these works did not consider improvements in carrier power.

Here, we present a method aimed at increasing the CNR of the beatnote signal in a CLaDS system through use of a strong optical local oscillator (LO) to boost the carrier power. To do this, an additional LO channel has been incorporated into the system in conjunction with additional frequency mixing of the received RF beatnote signal to extract the CLaDS spectra. In Fig. 1(a) the optical configuration for heterodyne-enhanced (HE) CLaDS using a DSB approach is detailed. The output from a chirped laser is split using a fiber-coupler [acting as a 1:2 splitter (FC)] into two arms, forming the LO channel and sample channels. The sample channel follows the original CLaDS system architecture [3], where an intensity modulator (or frequency shifter) is used to generate a multifrequency beam with known frequency spacing,  $\Omega$ . These co-propagating frequencies interact with the sample under test, and the sample's dispersion profile is encoded into the time-varying frequency of the heterodyne beatnote. In the LO channel, a frequency-shifter is used to enable optical heterodyne detection. In our prototype system, an optical delay line is used to create a difference in path lengths ( $L_1 \neq L_2$ ) between the LO and sample channels. This results in an effective shift of the original laser frequency by a fixed amount related to the chirp rate and effective path length difference,  $\Omega_{\text{LO}} = S \cdot \Delta L/c$ , where  $S$  is the chirp rate of the laser (Hz/s),  $\Delta L$  is the difference in path length (m), and  $c$  is the speed of light in the fiber (m/s). A neutral density filter (NDF) attenuating by  $\sim 30$  dB is placed in the signal path to mimic attenuation of the signal beam in the remote sensing configuration. The two channels are then recombined using a beam splitter (BS) and are heterodyne mixed on the photodetector (PD).

The resulting beatnote photocurrent contains the conventional CLaDS beatnote generated by the multiple frequencies in the sample channel (at  $\Omega$ ) as well as the beatnotes between

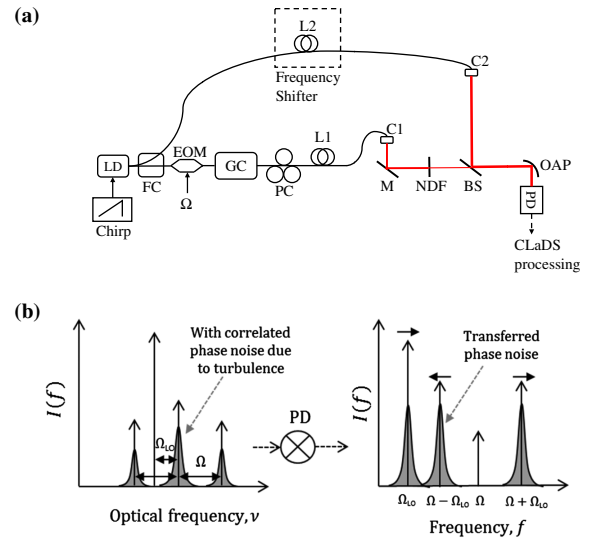


**Fig. 1.** (a) Implementation of the HE-enhanced CLaDS technique for in-lab free space measurements with a frequency-shifted LO generated using a fiber delay line. (b) Optical spectrum using dual-sideband CLaDS and an LO frequency shift less than the frequency offset ( $\Omega_{\text{LO}} < \Omega$ ). The resulting difference frequency spectrum after mixing on the photodetector is shown. The anti-correlated signals at  $\Omega - \Omega_{\text{LO}}$  and  $\Omega + \Omega_{\text{LO}}$  are used in further analysis to extract spectroscopic information from the sample.

each of those sample frequencies and the LO. Limited by the bandwidth of the photodetector, only difference frequencies are present in the signal after the square-law detection. The conversion of optical frequencies to RF beatnote signals is schematically shown in Fig. 1(b). Depending on the relationship between the magnitudes of  $\Omega_{\text{LO}}$  and  $\Omega$ , the turbulence-related phase noise in the LO beatnotes (i.e., beatnotes at  $\Omega_{\text{LO}} \pm \Omega$ ) is either correlated (for  $\Omega_{\text{LO}} > \Omega$ ) or anticorrelated (for  $\Omega_{\text{LO}} < \Omega$ ). In either case, the heterodyne-enhanced spectroscopic signal is extracted through remixing the RF beatnote signal by frequency doubling. In this first demonstration, the noise is anti-correlated and mitigated by frequency demodulating at the sum frequency at  $(\Omega + \Omega_{\text{LO}}) + (\Omega - \Omega_{\text{LO}}) = 2\Omega$ .

The nonlinear mixing can be performed in the analog domain using a combination of a notch filter (for the beatnote at  $\Omega$ ) and a frequency mixer or, as shown below, using analog downconversion, digitalization, and digital signal processing. In Fig. 2, this latter processing scheme is outlined, where the generated beatnote photocurrent is downconverted to the baseband (by mixing with  $\Omega$ ), and the resulting in-phase ( $I$ ) and quadrature ( $Q$ ) components are digitized. This complex digital signal is then high-pass filtered to remove the original signal at  $\Omega$ , and subsequently frequency-doubled to generate the equivalent sum frequency of LO RF beatnotes at  $2\Omega$ .

This initial demonstration of HE-CLaDS utilized a fiber-coupled diode laser operating around 1650 nm. The distributed feedback diode laser was used to target the R4 transition in a  $2\nu_3$  overtone band of methane around 1651 nm. A  $\sim 6$  m difference in effective length between the LO and signal channels in conjunction with a laser chirp of 250 MHz/ $\mu\text{s}$  generated an effective frequency shift of  $\Omega_{\text{LO}} \approx 7$  MHz. The signal

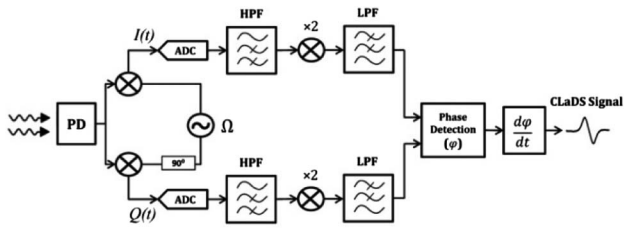


**Fig. 2.** Detection scheme for HE-CLaDS. PD, photodetector; ADC, analog to digital converter; HPF, high-pass filter; LPF, low-pass filter.

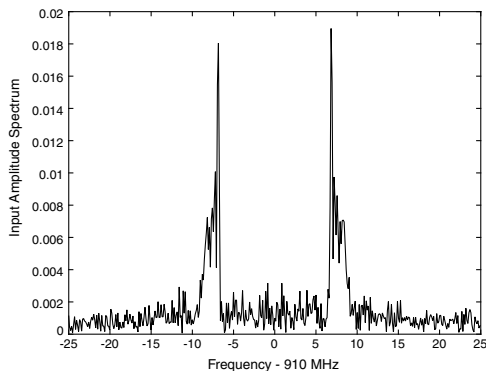


**Fig. 3.** Spectrum of the input signal downconverted at  $\Omega = 910$  MHz, showing the LO sideband beatnotes. Phase noise in these LO sideband beatnotes broadens their widths and is anti-correlated with respect to one another. Not shown here is the LO carrier beatnote, which lies outside the detection system bandwidth.

channel is operated using DSB CLaDS with an EOM driven by an RF sine wave at  $\Omega = 910$  MHz [7]. The PD photocurrent was then captured using a benchtop spectrum analyzer (Rhode & Schwartz FSW26), which downconverted the input time-domain signal (at  $\Omega$ ) and digitized the corresponding time-varying  $I$ ,  $Q$  signals. The spectrum of this input signal is presented in Fig. 3 and corresponds to the illustration shown in Fig. 1(b). With the attenuation set by NDF, the original CLaDS beatnote (at DC) is buried under noise and is not visible in the measured RF spectrum.

The complex, digital signal is then digitally bandpass filtered to limit noise and remove the direct DSB beatnote at  $\Omega$ , which is not enhanced by the LO. The spectrum at this stage is shown in Fig. 4(a). This filtered signal is then self-multiplied (squared), generating both sum and difference frequency signals. Through the mixing process, the anti-correlated phase noise is removed by the sum frequency generation, which is an effect that can be seen in the beatnote widths of 520 kHz in Fig. 4(a) reduced to 120 kHz in Fig. 4(b), which is comparable with that of conventional CLaDS. This also emphasizes the importance of removing the original beatnote frequency at 910 MHz. Even though in this experiment the original beatnote is buried under noise, the nonlinear mixing of the unfiltered input signal could result in the interference of the frequency-doubled original beatnote ( $2\Omega$ ) and the useful signal extracted as the sum frequency of the LO-enhanced beatnotes ( $(\Omega + \Omega_{LO}) + (\Omega - \Omega_{LO}) = 2\Omega$ ). Removal of the

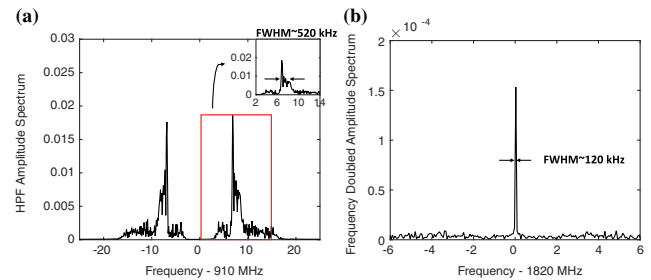


**Fig. 4.** (a) Spectrum after bandpass filtering to remove the original DSB CLaDS beatnote at  $\Omega$ . The inset highlights the phase-noise-induced broadening of the LO-enhanced beatnotes, with an FWHM measuring 520 kHz in the results presented here. (b) Sum frequency signal spectrum after digital square-law detection showing a clear reduction in the observed phase noise with a FWHM of 120 kHz.

conventional CLaDS beatnote at  $\Omega$  with straightforward notch filtering (either in the analog or digital domains) prevents this spectral interference.

After nonlinear mixing, the resulting sum frequency signal is frequency demodulated to reveal the HE-CLaDS spectra, an example of which is shown in Fig. 5. A comparison to conventional DSB CLaDS configuration is performed by acquiring a spectrum with all the available optical power directed into the signal channel [without splitters (FC and BS) in Fig. 1(a)], and the same attenuation [NDF in Fig. 1(a)] as the one used in the HE-CLaDS configuration. The CNR of the demodulated beatnote is 34 dB and 23 dB for HE-CLaDS and DSB CLaDS, respectively. This results in a standard deviation of the CLaDS spectrum fit residuals of 373 Hz for HE-CLaDS and 844 Hz for DSB CLaDS. In the DSB CLaDS configuration presented here, the sample dispersion is probed at twice the frequency used to drive the EOM (i.e.,  $2\Omega$ ). In a conventional DSB CLaDS system, this results in a reduction in signal amplitude by a factor of 2, due to the effective averaging of two beatnotes (carrier+upper sideband, carrier+lower sideband) at the same RF frequency [7]. The HE-CLaDS signal is extracted from the difference in only the sideband signals (spaced at  $2\Omega$ ), effectively creating a single-sideband (SSB) measurement scheme. As a result, the reduction by a factor of 2 present in conventional DSB CLaDS systems is avoided, which represents an advantage for HE-CLaDS. As illustrated in Fig. 5,

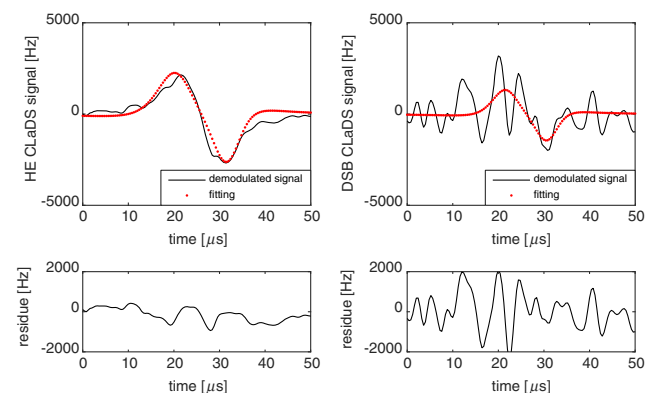


**Fig. 5.** CLaDS spectrum of methane around 1651 nm measured using the HE-CLaDS (left) and conventional DSB CLaDS (right).

a single spectral point SNR is thus a factor of  $\sim 4$  higher for HE-CLaDS. It should be noted that the baseline of small slope in the HE-CLaDS is caused primarily by phase noise cross talk between the two beatnotes enhanced by the LO, which is expected to be suppressed by creating a larger spacing between the beatnotes (currently limited by the used hardware and length of the delay line). The fringe-like pattern is due to lack of optical isolation in this proof-of-concept study. Therefore, a proper path length difference and optical isolation in the delay-line-based LO channel or another frequency-shifter technology should be considered to achieve optimal performance.

A proof-of-concept demonstration of a HE-CLaDS system is presented. This technique allows for heterodyne enhancement of weak signals received by the detector while preserving turbulence-induced phase noise immunity achieved through subsequent nonlinear mixing of LO-enhanced beatnote signals originating from two co-propagating waves. A factor of 2 increase in amplitude of the measured signal is observed, which mitigates the issue of intensity-dependent frequency averaging observed in DSB CLaDS [7]. We also have shown a factor of 2 decrease in measured noise achieved in HE-CLaDS via the LO enhancement of CNR, which, in combination with aforementioned signal increase, results in  $4\times$  higher SNR. It should be noted here that, even though the comparison assumes conserved total optical power in the current single-laser HE-CLaDS setup, the strong LO also can be generated using a second laser source, which would eliminate the problem of power budget optimization. Moreover, in the current HE-CLaDS test setup, half of the received optical power is lost in the unused optical beam created by the beam splitter, which ideally can be recovered with a second detector in a balanced detection system. Therefore, higher enhancement is potentially achievable in optimized HE-CLaDS systems. This result highlights the potential for remote sensing systems where turbulence-induced noise may limit sensor performance. While the demonstration here uses near-infrared technology, we expect this technique to be applicable to other spectral regimes. Also, the system presented here utilized a simple delay approach to generate an effective frequency shift in the LO channel. While easy to implement, this method to generate  $\Omega_{LO}$  can introduce additional noise due to chirp nonlinearity and the interferometric

configuration. Alternatively, an acousto-optic modulator (AOM) can be used to directly generate the LO frequency shift or a second frequency-locked laser source. Studies in the use of an AOM in the LO channel, the system noise contributions as compared with the delay method, and a quantitative comparison between the sensitivities in the HE-CLaDS and the conventional approach are currently ongoing and will be published elsewhere.

**Funding.** U.S. Department of Energy (DOE) (DE-FE0029059).

**Acknowledgment.** The authors would like to acknowledge financial support by the DoE NETL and from a generous contribution by Lynn and Thomas Ou.

<sup>†</sup>These authors contributed equally to this work.

## REFERENCES

1. P. Martín-Mateos and P. Acedo, *Opt. Express* **22**, 15143 (2014).
2. G. B. Rieker, F. R. Giorgetta, W. C. Swann, J. Koffler, A. M. Zolot, L. C. Sinclair, E. Baumann, C. Cromer, G. Petron, C. Sweeney, P. P. Tans, I. Coddington, and N. R. Newbury, *Optica* **1**, 290 (2014).
3. G. Wysocki and D. Weidmann, *Opt. Express* **18**, 26123 (2010).
4. F. R. Giorgetta, G. B. Rieker, E. Baumann, W. C. Swann, L. C. Sinclair, J. Koffler, I. Coddington, and N. R. Newbury, *Phys. Rev. Lett.* **115**, 103901 (2015).
5. M. Nikodem and G. Wysocki, *Opt. Lett.* **38**, 3834 (2013).
6. M. Nikodem, G. Plant, D. Sonnenfroh, and G. Wysocki, *Appl. Phys. B* **119**, 3 (2015).
7. M. Nikodem, G. Plant, Z. Wang, P. Prucnal, and G. Wysocki, *Opt. Express* **21**, 14649 (2013).
8. A. B. Carlson and P. B. Crilly, *Communication Systems: An Introduction to Signals and Noise in Electrical Communication*, 5th ed. (McGraw-Hill, 2010).
9. G. Plant, A. Hangauer, and G. Wysocki, in *Conference on Lasers and Electro-Optics (CLEO)*, OSA Technical Digest (Optical Society of America, 2015), paper SM10.2.
10. G. Plant, A. Hangauer, and G. Wysocki, *IEEE J. Sel. Top. Quantum Electron.* **23**, 147 (2017).
11. A. Hangauer and G. Wysocki, in *Conference on Lasers and Electro-Optics (CLEO)*, OSA Technical Digest (Optical Society of America, 2014), paper SM4E.5.
12. P. Martín-Mateos, B. Jerez, and P. Acedo, *Opt. Lett.* **39**, 2611 (2014).

# Heterodyne Efficiency in Chirped Laser Dispersion Spectroscopy

Yifeng Chen<sup>1</sup>, Genevieve Plant<sup>1,2</sup>, Gerard Wysocki<sup>1\*</sup>

<sup>1</sup>Electrical Engineering Department, Princeton University, Princeton, NJ, 08544, USA

<sup>2</sup>Electrical and Computer Engineering Department, University of Michigan, Ann Arbor, MI, 48109, USA  
email: \*gwysocki@princeton.edu

**Abstract:** We present an analysis of diffusive reflection and its effect on heterodyne efficiency in conventional and heterodyne-enhanced chirped laser dispersion spectroscopy motivated by applications in stand-off chemical detection.

**OCIS codes:** (300.6480) Spectroscopy, speckle; (300.6310) Spectroscopy, heterodyne; (300.6340) Spectroscopy, infrared

## 1. Introduction

Chirped laser dispersion spectroscopy, also known as CLaDS, is able to extract molecular dispersion information by frequency demodulating the heterodyne beatnote formed by multiple co-propagating optical frequencies through the sample [1]. The phase noise (due to atmospheric turbulence or scattering) is correlated between the probing waves and is effectively cancelled out by heterodyne detection, which makes the technique suitable for remote atmospheric gas sensing [1]. It was also found experimentally that the noise characteristic of CLaDS signal does not change significantly when the light is reflected off a rough surface, and only the return power is reduced due to scattering or diffused reflection [1]. We have recently proposed a solution to compensate for the power loss in the field by using a strong optical local oscillator (LO) to heterodyne beat with the returned probing waves [2]. The CLaDS turbulence- or scattering-induced phase noise cancellation property is preserved in the Heterodyne-Enhanced CLaDS (HE-CLaDS) technique, which additionally enhances the beatnote power via heterodyne mixing with a strong LO. However, it is important to investigate the impact on the heterodyne efficiency of the process if the probing beam reflects off a rough scattering surface. Here we present a theoretical analysis of the heterodyne efficiency in CLaDS as light reflects off a diffusive target. We show that under certain conditions the reduction of heterodyne efficiency in HE-CLaDS can be compensated by a LO of reasonable power.

## 2. Cross correlation between optical fields in CLaDS

It is well understood that when light is reflected off a rough surface whose roughness is on the same order as the wavelength, wavefronts of the reflected light are distorted and speckle patterns are formed at the detection plane [3]. Such speckles often introduce non-negligible noise to a heterodyne detection based system [3,4]. If we assume the vertical roughness fluctuation as a random variable, we find the cross correlation of the complex amplitudes of two optical fields with different wavelengths (wavenumbers) to be as following:

$$\langle \mu_{1,2} \rangle = \frac{\langle \mu_{1,2} \rangle}{\sqrt{|\langle \mu_{1,2} \rangle|} \sqrt{|\langle \mu_{1,2} \rangle|}} \quad (1)$$

Under ideal condition, the cross-correlation  $\mu_{1,2}$  is close to unity everywhere, corresponding to a heterodyne efficiency  $\eta_{\text{het}}$  of 100%. In conventional CLaDS, both fields are propagating collinearly and reflect off the same spot on the rough surface.

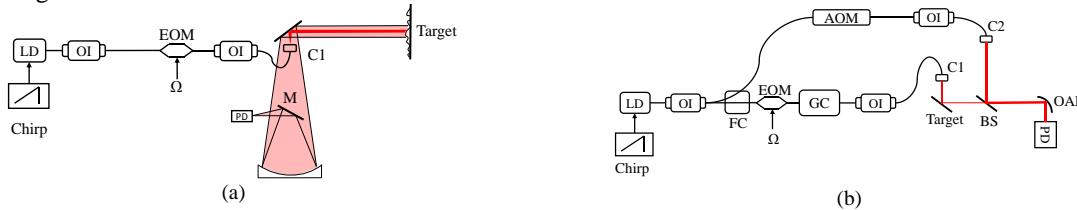


Figure 1. (a) Simplified CLaDS based remote sensing configuration; PD – photodetector, OI- optical isolator, EOM-electro-optic modulator, C1-collimator. The reflecting surface is optically rough for wavelength around 1650 nm. (b) Simplified in-lab HE-CLaDS configuration. The AOM provides 200MHz frequency shift in LO branch. The target is tested with both mirror and rough aluminum surface.

The frequency spacing in CLaDS is typically 1GHz, corresponding to  $\Delta\lambda \approx 0.009$  nm at 1650 nm [1]. Assuming the standard deviation of the height variation  $\sigma_h$  is on the same order of the wavelength, a small  $\Delta\lambda$  leads to cross-correlation of unity at the scattering plane [3]. At the detection plane,  $\mu_{1,2}$  is additionally determined by spatial correlation  $\tau_c$  of the height fluctuation, illumination area on the rough surface and imaging geometry. Varying  $\tau_c$  from 20 $\mu$ m to 1mm for typical rough metallic surface, the magnitude of  $\mu_{1,2}$  of the propagated fields back at the detection plane is found to remain close to unity across a radius of 1 cm at the detection plane. Such close

correlation suggests that the two fields share very similar wavefronts, which is shown in the cancelled phase variation between the two fields in Figure 2.



Figure 2. (a) Simulated speckle pattern at the detection plane.  $\tau_c=1$  mm,  $\sigma_h = 1.65\mu\text{m}$ , propagation distance = 35 m, focus length of the telescope = 40 cm. (b) Phase difference between the distorted complex optical amplitudes with  $\Delta\lambda = 0.009$  nm. The standard deviation of the residue phase difference is around  $3e-4$  radians.

### 3. Heterodyne efficiency in HE-CLaDS

In a HE-CLaDS setup as shown in Figure 1 (b), the close to unity correlation no longer holds as the LO wavefront does not experience the same distortion as the probing beam. However, if the speckle size is much wider than the detector area, the drop of  $\eta_{\text{het}}$  is expected to be less than one order of magnitude. A preliminary experiment was performed to estimate the decrease in  $\eta_{\text{het}}$  caused by diffusive reflection by comparing the beatnote carrier power change. Three beatnotes at 200MHz, 710MHz and 1110 MHz are formed by LO and the probing frequencies, whereas the beatnote at 910MHz is the conventional CLaDS beatnote. Three measurements were performed using: 1) an optical quality mirror as a control group, 2) a rough aluminum surface as a scattering target, and 3) the mirror followed by an attenuator to estimate the heterodyne efficiency. By keeping the heterodyne-enhanced beatnotes in measurement 2) and 3) one can clearly observe a 20dB difference in the 910MHz beatnotes indicating higher  $\eta_{\text{het}}$  when the mirror is used as a target (due to minimal wavefront distortion). A 54% loss in  $\eta_{\text{het}}$  is estimated for the scattering aluminum surface, which is very promising given the high dynamic range of near-infrared photodetectors allows for application of high power LO (four times LO powerful can compensate for the reduction in  $\eta_{\text{het}}$ ).

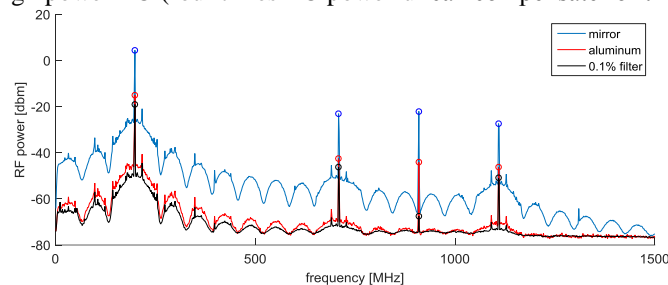


Figure 3. The RF spectra of the HE-CLaDS using a mirror and a piece of rough aluminum as reflective target. Relative  $\eta_{\text{het}}$  change due to scattering at aluminum surface is estimated to be 54% by referencing to the control group (blue spectrum).

### 4. Conclusion

We studied the heterodyne efficiency  $\eta_{\text{het}}$  in CLaDS when the probing beam reflects off a rough surface. The close correlation between wavefronts of the probing waves with small wavelength difference is predicted to yield high  $\eta_{\text{het}}$ , but significant attenuation within the sample channel suppresses an effective heterodyne gain. In HE-CLaDS, a strong LO can enhance the beatnote power efficiently, but  $\eta_{\text{het}}$  reduction due to wavefront mismatch is a limitation. Nonetheless when the photodetector size is matched to the expected speckle size, the  $\eta_{\text{het}}$  remains within 50% of the ideal case, which is an acceptable decrease if a powerful LO can be used to enhance the heterodyne gain. We will present an experimental validation of the wavefront cross-correlation models in CLaDS and HE-CLaDS and discuss practical implementations of the heterodyne enhancement technique to remote trace gas sensing.

**Acknowledgments:** The authors would like to acknowledge financial support by the DoE NETL grant # DE-FE0029059, from Princeton University and from a generous contribution by Lynn and Thomas Ou.

### 5. References

- [1] M. Nikodem, G. Plant, D. Sonnenfroh, and G. Wysocki, "Open-path sensor for atmospheric methane based on chirped laser dispersion spectroscopy," *Applied Physics B*, 119(1), pp.3-9 (2015).
- [2] G. Plant, Y. Chen, and G. Wysocki. "Optical Heterodyne-Enhanced Chirped Laser Dispersion Spectroscopy." CLEO: Science and Innovations. Optical Society of America, 2016.
- [3] J. Goodman. "Speckle phenomena in optics: theory and applications". Roberts and Company Publishers, 2007.
- [4] N.A. Macleod, R. Rose, and D. Weidmann. "Middle infrared active coherent laser spectrometer for standoff detection of chemicals." *Optics letters* 38.19 (2013): 3708-3711.